Int. J. Electrochem. Sci., 14 **(2019)** 1884 – 1896, doi: 10.20964/2019.02.09

International Journal of ELECTROCHEMICAL SCIENCE
www.electrochemsci.org

Preparation and Properties of Ni-W-rGO Composite Coatings

Bingying Wang[*], *Yi Ma, Chaofan Ran, Guodong Liu, Zhenbo Hou*

School of Mechanical and Electrical Engineering, China University of Petroleum, Qingdao 266580, China
[*]E-mail: tdwby2004@126.com

Received: 29 September 2018 / *Accepted:* 5 November 2018 / *Published:* 5 January 2019

Graphene oxide (GO) was prepared by a modified Hummers method. Ni-W-rGO composite coatings were synthesized by pulsed electrodeposition on an N80 steel plate. The GO specimens were characterized by Raman spectroscopy, Fourier-transform infrared spectroscopy, and X-ray diffraction. Microstructures of the Ni-W-rGO composite coatings were characterized by scanning electron microscopy equipped with energy dispersion spectroscopy analysis. The microhardness of all coatings were evaluated with a microhardness tester. The corrosion behavior of the Ni-W-rGO composite coatings was investigated by potentiodynamic polarization and electrochemical impedance spectroscopy in 3.5 wt% NaCl solution. The results showed that GO had been reduced to rGO on the cathode, forming a composite coating with nickel and tungsten co-deposits on the N80 plate. The coating was denser due to improved surface morphology, and GO markedly improved its microhardness and corrosion resistance. The optimum GO concentration was 0.6 g/L.

Keywords: composite coating; corrosion resistance; graphene oxide; microhardness; reduced graphene oxide

1. INTRODUCTION

Nickel-tungsten alloy coating is widely used in petroleum, petrochemical, and aerospace engineering because of its high melting point, high hardness, and good corrosion resistance [1-3]. Thus, nickel-tungsten alloy coating has gradually replaced toxic chromium plating to meet the requirements of the green production environment. However, as the equipment deteriorates with wear, the hardness and corrosion resistance of the nickel-tungsten alloy coating become less and less satisfactory for protection purposes.

Graphene was first synthetized in 2004 by scientists K.S. Novoselov and A.K. Geim from the University of Manchester [4]. The structure of graphene is an infinite plane of regular hexagonal

carbocyclic rings formed by sp^2 hybridization of carbon atoms. The rings are mechanically stable in the direction of the plane. Graphene, which has the strength of 130 GPa and Young's modulus of 1.0 TPa [5], is believed to be by far the strongest material discovered to date. Graphene is theoretically impermeable to all ions and molecules, which makes it an ideal corrosion-resistant material [6] capable of improving the properties of other materials.

However, because of its low density and lack of surface functional groups, graphene is poorly dispersible in aqueous solutions [7]. This hinders its use in electrodeposition, which requires adding a reinforcing phase into the plating bath to form a composite coating [8, 9]. In contrast, graphene oxide (GO) not only has all the excellent properties of graphene but also contains a large number of surface functional groups [10], such as hydroxyl, epoxy, carbonyl, or carboxyl. Graphene oxide has good solubility in water and forms stable and uniform aqueous dispersions [11-14]. This makes electrodeposition one of the most economical and technically feasible procedures for the synthesis of graphene/metal composites [15-17].

Graphene oxide is a prospective reinforcing phase for electrodeposition. It can improve the corrosion resistance of composite coatings [18] and enhance their smoothness and density [19]. Studies have shown that a moderate addition of GO can improve the thermal stability and Young's modulus of composite coatings [20]. Moreover, the addition of GO can increase the fracture toughness of composite coatings by a factor of 4 when compared with a pure hydroxyapatite coating [21]. Graphene oxide is currently used to produce various types of composite materials with polymers [22], minerals [21], and metals [23].

In this study, GO was prepared by a modified Hummers method, and Ni-W-rGO composite coatings were electrodeposited onto N80 steel plates. The structure of GO and graphene in composite coatings was analyzed by Raman spectroscopy, Fourier-transform infrared spectroscopy (FTIR), and X-ray diffraction (XRD), whereas composite coatings were analyzed by scanning electron microscopy (SEM) and energy-dispersive X-ray spectroscopy (EDS). The microhardness of the composite coatings was tested using a microhardness tester. The corrosion resistance was studied by observing electrochemical corrosion behavior in 3.5 wt% NaCl solution.

2. EXPERIMENTAL

2.1. Reagents

Ggraphite powder was obtained from Qingdao Tenghuida Graphite Technology Co., Ltd. (Qingdao, China), NH_3 from Yantai Sanhe Chemical Reagent Co., Ltd. (Yantai, China), $NiSO_4{\cdot}(H_2O)_6$ from Tianjin Dingsheng Chemical Co., Ltd. (Tianjin, China), and sodium citrate ($Na_3C_6H_5O_7$) from Tianjin Fucheng Chemical Reagent Factory (Tianjin, China). All other reagents were purchased from Sinopharm Chemical Reagent Co., Ltd. (Shanghai, China), including concentrated H_2SO_4 (98%), $KMnO_4$, $NaNO_3$, H_2O_2 HCl, Na_2WO_4, $NiCl_2{\cdot}6H_2O$, H_3BO_3, NaOH, Na_2CO_3, $Na_3PO_4{\cdot}12H_2O$, $Na_2SiO_3{\cdot}9H_2O$, and anhydrous ethanol. All chemicals used in this work were of the analytical grade.

2.2. Preparation of GO

Graphene oxide was synthesized by a modified Hummers method [24]. The reaction mixture was prepared by mixing 80 mL of concentrated H_2SO_4 (98 wt%) with 2 g of graphite powder (3000 mesh) and 1 g of $NaNO_3$ under constant stirring. Then, 12 g of K_2MnO_4 was added slowly into the continuously stirred mixture. After stirring for 2 h, the mixture was incubated for 0.5 h in a water bath at a constant temperature of 35 °C, after which 160 mL of distilled water was added to the mixture. After another 15 min, 500 mL of distilled water with a temperature of 80 °C was added to the mixture, followed by 30 mL of 30% H_2O_2. The mixture was filtered and washed twice with 5% HCl [25] and distilled water until the pH value reached 7. The resulting brown-black material was lyophilized to calculate the concentration of GO in the solution.

2.3. Electrodeposition

Ni-W-rGO composite coatings were prepared by pulse electrodeposition (SMD-10, Handan City Dashun Electroplating Equipment Factory, China). The process parameters and bath composition are shown in Table 1. A pure nickel plate (99.5%) was used as the anode, and an N80 steel plate (30 mm × 20 mm × 3 mm) as the cathode. Prior to electrodeposition, the selected side was pre-ground and polished, and the remaining five sides were sealed with silicone. To degrease the surface, the plates were first soaked into an alkaline solution containing 20 g/L of NaOH, 20 g/L of Na_2CO_3, 10 g/L of $Na_3PO_4 \cdot 12H_2O$, and 10g/L of $Na_2SiO_3 \cdot 9H_2O$ for 10 min and then rinsed with distilled water. The alkaline washing and processing of the cathode plate was followed by acid pickling in 5% H_2SO_4.

Table 1. Bath composition and electrodeposition conditions for the synthesis of Ni-W-rGO composite coatings.

$NiSO_4 \cdot 6H_2O$ (nickel sulfate)	50 g/L
$C_6H_5Na_3O_7 \cdot H_2O$(sodium citrate)	80 g/L
$Na_2WO_4 \cdot 2H_2O$(sodium tungstate)	60 g/L
$C_6H_4SO_2NNaCO \cdot 2H_2O$(sodium saccharin)	2 g/L
$NiCl_2 \cdot 6H_2O$ (nickel chloride)	10 g/L
Graphene oxide	0.2 g/L, 0.4 g/L, 0.6 g/L, 0.8 g/L, 1.0 g/L
Type of current	Pulse power
pH	7
Temperature (◦C)	60
Current density	1.5A/dm^2
Sonication	80 KHz,300 W

The pickled sample was then placed in a plating bath. Before electrodeposition (plating), the plating bath was stirred on an electromagnetic stirrer (DF-101S, Zhengzhou Yuhua Instrument Manufacturing Co., Ltd., China) at 600 rpm for 2 h and sonicated for 30 min (KQ-300VDB, Kunshan Ultrasonic Instrument Co., Ltd., China). The electrodeposition was performed for 2 h at an average current density of 1.5 A/dm^2 and controlled temperature of 60 °C. The bath was agitated with ultrasound

at a frequency of 80 KHz and power of 300 W. The electrodeposition was repeated with various concentrations of GO particles, namely 0.2 g/L, 0.4 g/L, 0.6 g/L, 0.8 g/L, and 1.0 g/L. A schematic diagram of the employed pulse electrodeposition system is shown in Figure 1.

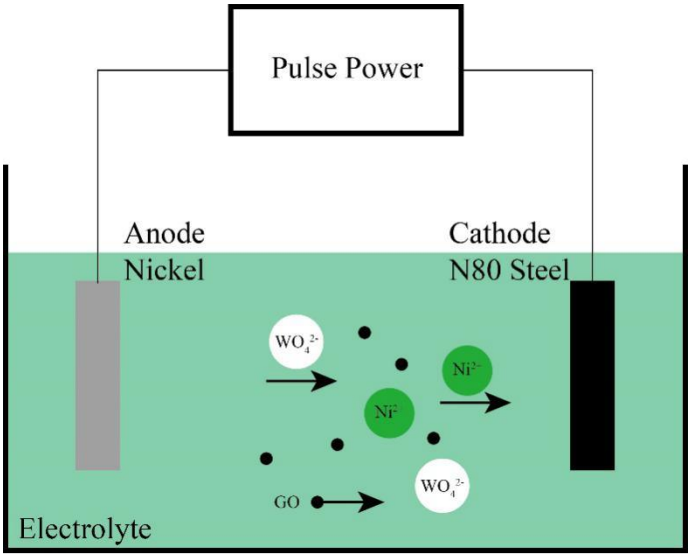

Figure 1. A schematic diagram of the pulse electrodeposition system used in this study.

2.4. Analysis and characterization

The phases of GO were characterized by Raman spectroscopy (DXR™2 Raman microscope, Thermo Fisher Scientific, Massachusetts, USA; 532 nm laser, 5 mV, 60-times scanning), FTIR (Nicolet iS50, Thermo Fisher Scientific; 4 cm^{-1}, 128-times scanning), and XRD (Cu-Kα radiation) operating at 40 kV and 250 mA over the 2θ range of 10–90°. The Ni-W-rGO composite coatings were also characterized using Raman spectroscopy and FTIR after the composite coating samples were immersed in 30% HNO_3 solution for 5 min. The surface morphologies of Ni-W-rGO composite coatings were researched using scanning electron microscope (Nova Nano SEM450, FEI Company, Oregon, USA) coupled with an EDS spectrometer.

The microhardness tester (HV-1000A, Laizhou Huayin Experimental Instrument Co., Ltd., China) was used to test the microhardness of the composite coating for 15 s at 200 gf. Five points were selected on the coating for testing, and the average value was taken as the microhardness value of the coating.

Electrochemical measurements were performed at room temperature using the CHI660D electrochemical workstation (CH Instruments, Inc., Texas, USA) and a typical three-electrode cell with 3.5% NaCl as the electrolyte. The setting of the electrochemical cell included a 1 cm^2 area of the deposited coating as the working electrode, carbon rod as the auxiliary electrode, and saturated calomel as the reference electrode. The open circuit potential was measured first, and the test was stopped when the open circuit potential amplitude was less than 10 mV in 400 s. Next, the potentiodynamic polarization curve was obtained by scanning the range from -250 mV to 250 mV (relative to the open circuit potential)

at a scan speed of 0.166 mV/s. Finally, the AC impedance measurements were performed in the frequency range from 10^5 Hz to 10^{-2} Hz. The starting potential was the measured open circuit potential.

3. RESULTS AND DISCUSSION

3.1. Characterization of GO

Figure 2 shows the basic characterization of GO. The Raman spectrum of carbon materials generally consists of several very strong characteristic peaks with wavenumbers in the range of 1000–2000 cm^{-1}, and a few other modulation structures. The slight changes in the intensity, shape, and position of the spectral peaks are related to the structural information of the carbon material [26]. Figure 2a shows the Raman spectrum of GO. The two distinct peaks at 1362 cm^{-1} and 1562 cm^{-1} are the characteristic D and G bands of GO [27]. D band, which is lower than G band, is caused by symmetrical stretching vibration (radial breathing pattern) of the sp^2 carbon atom in the aromatic ring and requires a defect to activate. The intensity of D band is usually used to measure the degree of disorder of the material structure. G band originates from the stretching vibration of sp^2 carbon atoms, which corresponds to the vibration of the E2g optical phonon in the center of the Brillouin zone [28].

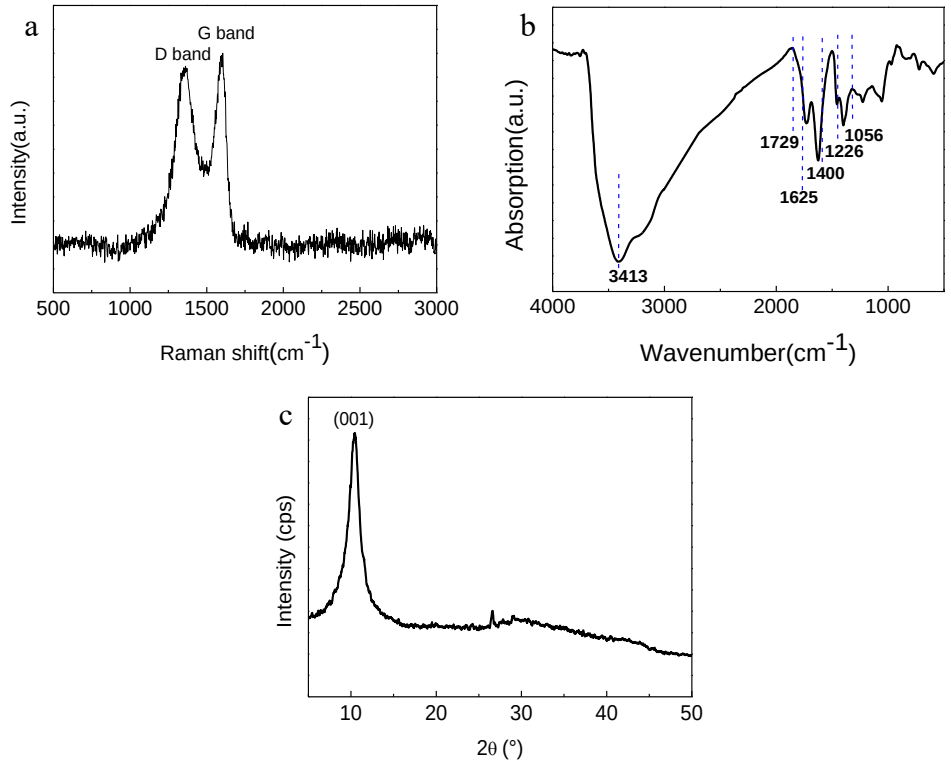

Figure 2. (a) Raman spectrum, (b) FTIR spectrum, and (c) XRD pattern of GO.

Infrared spectroscopy is mainly used to qualitatively characterize the chemical structure of graphene and its derivatives or composites. Figure 2b is the FTIR spectrum of GO, which displays the vibrational absorption peak of hydroxyl OH at 3413 cm^{-1}, deformation absorption peak of hydroxyl OH at 1400 cm^{-1}, and stretching vibration of carbonyl CO at 1729 cm^{-1}. The stretching vibration peak of epoxy CO can be observed at 1226 cm^{-1}, stretching vibration peak of alkoxy CO at 1056 cm^{-1}, and

deformation vibration peak at 1625 cm^{-1}. The presence of oxygen-containing functional groups not only proves that graphite was completely oxidized during the electrodeposition process, but also that GO was combined with the metal matrix. The XRD spectrum (Figure 2c) of GO has a peak near $2\theta = 11°$, which is the characteristic peak of GO [12]. This indicates that the prepared material was truly GO.

3.2. Characterization of Ni-W-rGO composite coating

To confirm the existence of a graphene sheet in the Ni-W-rGO composite coating, Raman and FTIR spectra of the coating were recorded after corroding it with 30% HNO_3 for 5 min. The Raman spectrum of the Ni-W-rGO composite coating after corrosion (Figure 3a) shows two evident characteristic peaks at 1306 cm^{-1} and 1559 cm^{-1}, which are shifted in comparison with the Raman spectrum of GO. This hypochromatic shift of D and G bands may also include a contribution from other functional groups, which increased the vibrational energy of GO. Characteristically of the reduction of GO, the intensity of D band was greater than the intensity of G band [29]. In addition, the intensity of D and G bands of Ni-W-rGO composite coatings was markedly increased in comparison to GO due to an increased concentration of defects in graphene nanosheets [30]. The FTIR spectrum of the composite coating after corrosion (Figure 3b) shows that the intensity of all characteristic peaks decreased, most notably the intensity of the vibrational absorption peak of hydroxyl OH at 3413 cm^{-1}. This provides evidence for the effectiveness of electrochemical reduction [31]. Together, the results of Raman and FTIR spectroscopy show that GO was reduced and co-deposited with Ni-W during the formation of the composite coating.

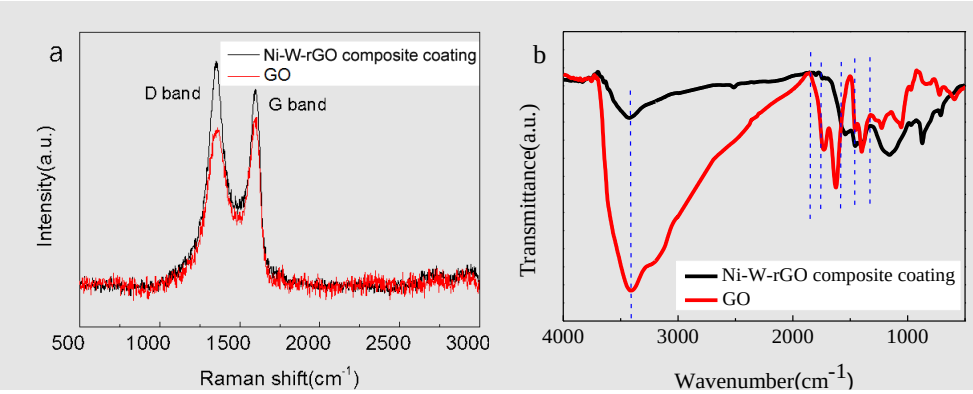

Figure 3. (a) Raman spectra, and (b) FT-IR spectra of GO and Ni-W-rGO composite coating.

The impact of GO on the morphology of Ni-W-rGO composite coatings can be observed in SEM micrographs obtained from the GO-coated composite coatings. Figures 4a-f show the surface morphology of the Ni-W alloy coating and Ni-W-rGO composite coatings. Figures 4b-f correspond to the characterized surfaces of Ni-W-rGO composite coatings for various concentrations of GO (0.2 g/L, 0.4 g/L, 0.6 g/L, 0.8 g/L and 1.0 g/L). As shown in Fig. 4a, the surface of the Ni-W-rGO composite coating was markedly different from the Ni-W alloy coating, demonstrating high roughness. This pinhole structure is the result of the interactions between GO layers after their reduction [32]. With the

increase of GO addition, the concentration of rGO, and in turn of the defects on the surface of metal crystals, also increases. The defects provide more numerous nucleation sites for nickel atoms [33, 34]. Also, the growth of the rGO film inhibits the continuous growth of nickel deposits and promotes the refinement of the grains [35]. In addition, the pinhole structure makes the composite coating conducive for ions in the plating bath, which then fill the defects in the pinhole structure and become densely deposited on the cathode plate.

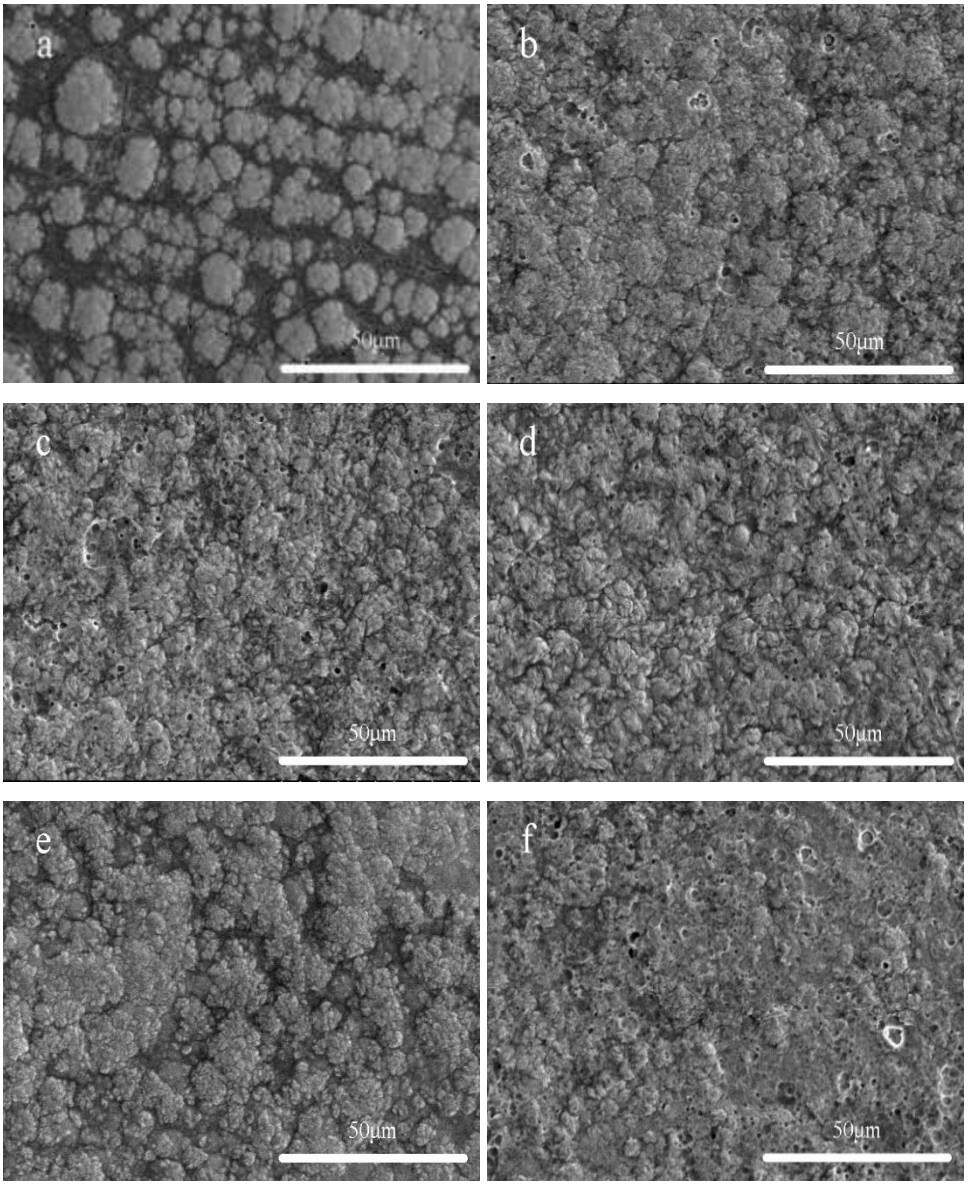

Figure 4. The surface morphology of deposits: (a) Ni-W, (b) Ni-W-rGO (0.2 g/L), (c) Ni-W-rGO (0.4 g/L), (d) Ni-W-rGO (0.6 g/L), (e) Ni-W-rGO (0.8 g/L), and (f) Ni-W-rGO (1.0 g/L).

When the concentration of GO was 0.6 g/L (Figure 4d), the particles were more even in size, evenly distributed on the composite coating surface, and formed relatively few clusters. Also, there were fewer bulges and cracks on the surface, making the composite coating flat and dense. When the concentration of GO was increased beyond 0.6 g/L, the amount of GO particles exceeded the holding

capacity of the plating bath and could not be completely dispersed in the solution. This caused the formation of numerous particle clusters, which increased the roughness of the composite coating surface and decreased its tightness and uniformity [36].

The SEM and EDS images of a cross-section of the composite coating are shown in Figure 5, which demonstrates no apparent pores or other defects. This is because the surface defects of rGO are continuously filled with metallic nickel and tungsten particles during deposition, making the composite coating relatively dense as a whole. The EDS results show that the composite coating mainly contains Ni, W, and C; the elemental atomic content changes with the different concentrations of GO, as shown in Figure 5b. With increasing concentration of GO in the plating bath, the content of carbon atoms in the coating gradually increases, the content of nickel atoms gradually decreases, and the content of tungsten atoms remains relatively constantly low. The increase of carbon content corresponds to an increased content of graphene deposited on the composite coating with increasing concentration of GO in the plating solution.

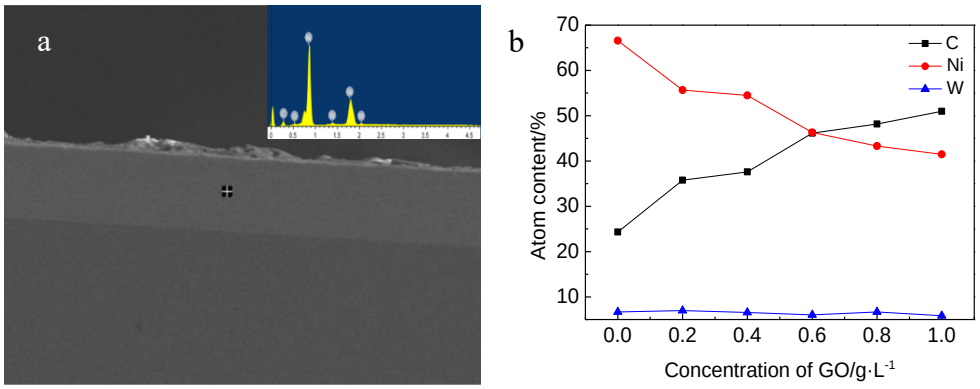

Figure 5. (a) SEM and (b) EDS images of the cross-section of the Ni-W-rGO composite coating.

3.3. Microhardness of the coatings

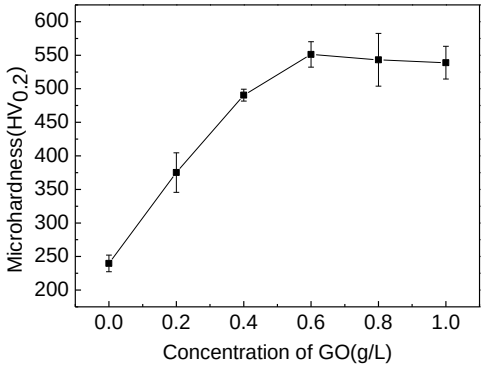

Figure 6. Microhardness of composite coatings at various concentrations of GO (vertical error bars represent variance).

Microhardness of the composite coating is presented in Figure 6. When the concentration of GO increased from 0 g/L to 0.2 g/L, the microhardness of the composite coating notably increased (from 231.16 $HV_{0.2}$ at 0 g/L to 375.12 $HV_{0.2}$ at 0.2 g/L of GO), indicating that the addition of GO can significantly improve the microhardness of the Ni-W alloy coating. Increased GO concentration increases the probability of rGO deposition onto the substrate surface, which increases the number of nucleation sites. Crystal growth is inhibited, grains become refined, and the number of coating defects is reduced. The dislocation pile-ups at grain boundaries impede the motion of dislocations, which results in an increased microhardness of the composite coating [37]. The maximum microhardness of 551.14 $HV_{0.2}$ was reached when the concentration of GO particles in the bath was 0.6 g/L. As the concentration of GO increased further, excess particles started to form clusters, and the microhardness decreased accordingly. The optimum concentration of GO for enhanced microhardness was thus found to be 0.6 g/L.

3.4. Electrochemical corrosion behavior of coatings

The differences in corrosion resistance of GO and Ni-W-rGo were studied by AC-impedance and polarization measurements at various concentrations of GO in 3.5% NaCl medium. Figure 7a shows the corresponding Nyquist plots for the measured samples, and the inset illustrates the equivalent circuit model proposed for the coating system. Figure 7a shows that the corrosion resistance of the coatings was markedly improved, irrespectively of the concentration of GO particles added into the plating bath. Because of good conductivity, rGO provides an alternative path for the electron transfer, bypassing the transfer from the anode to the cathode through the metal layer. In this way, rGO prevents the corrosive medium from reaching the substrate and makes the Ni-W-rGo composite coating more resistant to corrosion in comparison to the Ni-W alloy coating.

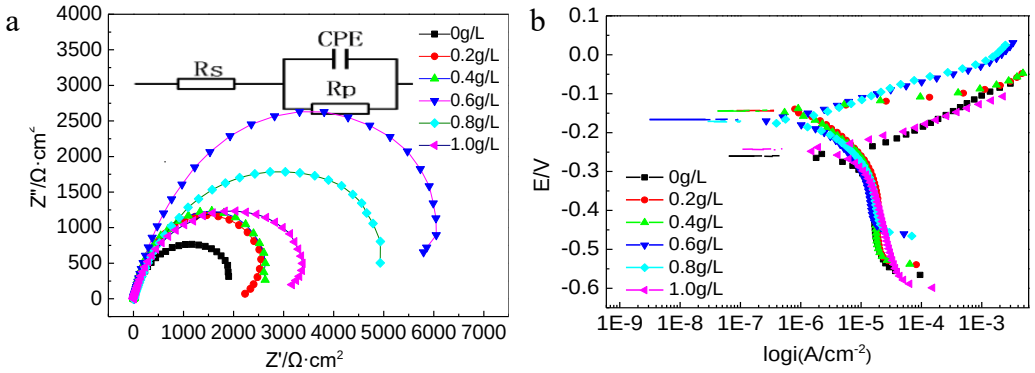

Figure 7. (a) Nyquist plots. The inset illustrates is the equivalent circuit model proposed for the coating system. Rs is the solution resistance, CPE is the normal phase component between the solution and the coating, and Rp is the electrochemical reaction charge transfer resistance. (b) Polarization curves of the coatings in 3.5 wt% NaCl solution.

Figure 7 also demonstrates that the impedance spectrum is single-capacitive. When there is no rGO in the plating solution, the capacitive arc radius of the alloy coating is the smallest, and the corrosion resistance is the poorest. With the addition of rGO, the corrosion resistance of the composite coating is significantly enhanced. As indicated by the largest arc radius of the impedance spectrum, the corrosion resistance of the composite coating was the highest when the concentration of GO in the bath was 0.6 g/L.

The corrosion kinetic parameters of the coatings were determined by an equivalent circuit model. The refined fit parameters for each coating sample are summarized in Table 2. Compared with Ni-W alloy coatings, the charge transfer resistance of the Ni-W-rGO composite coatings was markedly increased, irrespectively of the concentration of GO particles added to the plating bath. Generally, the Rp values of the coatings increased up to 0.6 g/L of GO in the plating bath, which indicates that the charge transfer was most difficult at this concentration [38]. Moreover, at 0.6 g/L of GO, CPE reached the lowest value of 0.0001604 Ω^{-1} cm^{-2} s^{-n}, whereas the Ni-W-rGO composite coatings exhibited the maximum charge transfer resistance of 7010 Ω cm^2. According to the formula Lex = $\varepsilon_0 \bullet \varepsilon_r$ / CPE (Lex is the space charge layer thickness of oxide, ε_0 is the vacuum dielectric constant, ε_r is the corrosion product film of Fe at room temperature Relative permittivity), the products layer of corrosion is the thickest, which is the best protection for the substrate, the corrosion resistance of the composite coating is the best.

Table 2. AC-impedance parameters of Ni-W and Ni-W-rGO composite coatings.

The concentration of GO (g/L)	R_s ($\Omega \bullet cm^2$)	R_p ($\Omega \bullet cm^2$)	CPE-T ($\Omega^{-1}cm^{-2}s^{-n}$)	CPE-P ($\Omega^{-1}cm^{-2}s^{-n}$)
0	3.743	2320	0.0007658	0.74007
0.2	3.059	2877	0.0004349	0.87063
0.4	4.321	2969	0.0008535	0.87474
0.6	3.96	7010	0.0001604	0.82223
0.8	3.194	5677	0.0002179	0.71596
1.0	3.538	3781	0.0001646	0.74517

The polarization curves for Ni-W alloy coating and Ni-W-rGO composite coatings at different concentrations of GO are shown in Figure 7b. The corrosion test was performed in 3.5 wt% NaCl solution, and the values of corrosion potential and current density were obtained using Tafel plot. The refined fit parameters for each coating sample are summarized in Table 3. I_{corr} is the corrosion current density, which represents the corrosion rate. E_{corr} is the corrosion potential, indicating the corrosion tendency.

The I_{corr} value was 1.08×10^{-6} when the concentration of GO was 0.2 g/L, which is lower than the I_0 value of 2.06×10^{-6} of the Ni-W alloy coating. The I_{corr} value of the coatings decreased up to 0.6 g/L

of GO in the plating bath and reached the minimum value of 5.14×10^{-7}, whereas E_{corr} increased proportionally with the increasing concentration of GO. Because of the good conductivity of rGO, the increased content of rGO in the composite coating provides an additional path for electron transfer. By preventing the prolonged exposure of underlying substrates to corrosive environments, the addition of GO particles can significantly enhance the corrosion resistance of composite coatings [39].

Table 3. Electrochemical parameters of the coatings obtained from the polarization test.

The concentration of GO (g/L)	B_a (mV/decade)	B_c (mV/decade)	I_{corr} (A/cm^2)	E_{corr} (mV)
0	27	-40	2.06E-06	-261
0.2	12	-107	1.08E-06	-138
0.4	15	-104	9.43E-07	-140
0.6	43	-43	5.14E-07	-166
0.8	57	-62	9.49E-07	-174
1.0	41	-105	3.27E-06	-143

However, with the further increase of GO concentration, the corrosion current density gradually increased, which may be due to a too high content of GO in the plating bath. When the plating bath contains excess GO particles, they form clusters, and the probability of collision among them on the cathode increases. This increases the surface defects of composite coating, and the corrosion resistance correspondingly declines. Regarding the magnitude of the corrosion parameters, the optimum concentration of GO was 0.6 g/L, which is consistent with the conclusions of the AC impedance experiments.

4. CONCLUSIONS

Ni-W-rGO composite coatings with a compact substrate surface and uniform structure were successfully prepared on an N80 steel surface. The coatings were tested for morphology, composition, microhardness and corrosion properties. The results of Raman spectroscopy, FTIR, and XRD show that the preparation of GO was successful. Raman spectroscopy and FTIR also showed that GO was reduced to rGO during the electrodeposition process. The results of EDS confirmed the existence of graphene in the composite coatings, whereas SEM showed that the surface roughness of the composite coating increased with the addition of rGO. The microhardness test demonstrated that the microhardness of the Ni-W-rGO composite coatings increased compared with the Ni-W alloy coating. Electrochemical corrosion tests showed that the corrosion resistance of the composite coating was enhanced by the

addition of GO. With the increase of GO content, the hardness and corrosion resistance of the composites first increased and then decreased. The optimum concentration of GO for enhanced microhardness and corrosion resistance was found to be 0.6 g/L.

ACKNOWLEDGMENTS

The authors gratefully acknowledge the Taishan Scholar Foundation (ts201511018) and the Fundamental Research Funds for the Central Universities (18CX05002A).

References

1. J. Xu, J. Tao, S. Jiang, Z. Xu, *Appl. Surf. Sci*., 254 (2008) 4036.
2. Q. Zhao, Y. Liu, E.W. Abel, *Appl. Surf. Sci*., 240 (2005) 441.
3. S. Zhou, X. Zeng, Q. Hu, Y. Huang, *Appl. Surf. Sci.*, 255 (2008) 1646.
4. K.S. Novoselov, A.K. Geim, S.V. Morozov, D. Jiang, Y. Zhang, S.V. Dubonos, I.V. Grigorieva, A.A. Firsov, *Science*, 306 (2004) 666.
5. C. Lee, X. Wei, J.W. Kysar, J. Hone, *Science*, 321 (2008) 385.
6. V. Berry, *Carbon*, 62 (2013) 1.
7. A. Siokou, F. Ravani, S. Karakalos, O. Frank, M. Kalbac, C. Galiotis, *Appl. Surf. Sci.*, 257 (2011) 9785.
8. H. He, C. Gao, *Chem. Mater*., 22 (2010) 5054.
9. T. Ramanathan, A.A. Abdala, S. Stankovich, D.A. Dikin, M. Herrera-Alonso, R.D. Piner, D.H. Adamson, H.C. Schniepp, X. Chen, R.S. Ruoff, S.T. Nguye, I.A. Aksay, R.K. Prud'Homme, L.C. Brinson, *Nat. Nanotechnol*., 3 (2008) 327.
10. L. Chen, S. Chai, K. Liu, N. Ning, J. Gao, Q. Liu, F. Chen, Q. Fu, *Acs. Appl. Mater. Inter*., 4 (2012) 4398.
11. S.J. An, Y. Zhu, H.L. Sun, M.D. Stoller, T. Emilsson, S. Park, A. Velamakanni, J. An, R.S. Ruoff, *J. Phys. Chem. Lett*., 1 (2010) 1259.
12. H.L. Guo, X.F. Wang, Q.Y. Qian, F.B. Wang, X.H. Xia, *Acs. Nano*, 3 (2009) 2653.
13. Y. Shao, J. Wang, M. Engelhard, C. Wang, Y. Lin, *J. Mater. Chem*., 20 (2010) 743.
14. M. Zhou, Y. Wang, Y. Zhai, J. Zhai, W. Ren, F. Wang, S. Dong, *Chemistry*, 15 (2009) 6116.
15. S.A. Lajevardi, T. Shahrabi, *Appl. Surf. Sci.*, 256 (2010) 6775.
16. E. Rudnik, L. Burzyńska, Ł. Dolasiński, M. Misiak, *Appl. Surf. Sci*., 256 (2010) 7414.
17. H. Yang, X. Guo, N. Birbilis, G. Wu, W. Ding, *Appl. Surf. Sci*., 257 (2011) 9094.
18. Z. Yu, H. Di, Y. Ma, L. Liang, P. Yang, C. Zhang, Y. He, *Appl. Surf. Sci*., 351 (2015) 986.
19. M.Y. Rekha, A. Kamboj, C. Srivastava, *Thin. Solid. Films*, 636 (2017) 593.
20. S. Qi, X. Li, Z. Zhang, H. Dong, *Thin. Solid. Films*, 644 (2017) 106.
21. Y. Liu, Z. Dang, Y. Wang, J. Huang, H. Li, *Carbon*, 67 (2014) 250.
22. S. Stankovich, D.A. Dikin, G.H. Dommett, K.M. Kohlhaas, E.J. Zimney, E.A. Stach, R.D. Piner, S.T. Nguyen, R.S. Ruoff, *Nature*, 442 (2006) 282.
23. A. D. Moghadam, E. Omrani, P. L. Menezes, P. K. Rohatgi, *Composites. Part. B*, 77 (2015) 402.
24. N.M.R. Peres. Neto, *Vacuum*, 83 (2009) 1248.
25. C.M.P. Kumar, T.V. Venkatesha, R. Shabadi, *Mater. Res. Bull*., 48 (2013) 1477.
26. D.A. Dikin, S. Stankovich, E.J. Zimney, R.D. Piner, G.H. Dommett, G. Evmenenko, S.T. Nguyen, R.S. Ruoff, *Nature*, 448 (2007) 457.
27. J. Chen, J. Li, D. Xiong, Y. He, Y. Ji, Y. Qin, *Appl. Surf. Sci*., 361 (2016) 49.
28. F. Tuinstra, J.L. Koenig, *J. Chem. Phys.,* 53 (1970) 1126.
29. E. Casero, A.M. Parra-Alfambra, M.D. Petit-Domínguez, F. Pariente, E. Lorenzo, C. Alonso,

Electrochem. Commun., 20 (2012) 63.
30. D. Kuang, L. Xu, L. Liu, W. Hu, Y. Wu, *Appl. Surf. Sci*., 273 (2013) 484.
31. S. Liu, J. Wang, J. Zeng, J. Ou, Z. Li, X. Liu, S. Yang, *J. Power. Sources*, 195 (2010) 4628.
32. W. Lv, D.M. Tang, Y.B. He, C.H. You, Z.Q. Shi, X.C. Chen, C.M. Chen, P.X. Hou, C. Liu, Q.H. Yang, *Acs. Nano*, 3 (2009) 3730.
33. M. Stroumbouli, P. Gyftou, E.A. Pavlatou, N. Spyrellis, *Surf. Coat. Tech.*, 195 (2005) 325.
34. Y.J. Xue, H.B. Liu, M.M. Lan, X.C. Ku, J.S. Li, *Chin. J. of Nonferrous. Met*., 20 (2010) 1599.
35. Z. Xue, W. Lei, Y. Wang, H. Qian, Q. Li, *Surf. Coat. Tech*., 325 (2017) 417.
36. Y.J. Mai, M.P. Zhou, H.J. Ling, F.X. Chen, *Appl. Surf. Sci*., 433 (2018) 232.
37. C. Liu, F. Su, J. Liang, *Appl. Surf. Sci*., 351 (2015) 889.
38. Y. Fan, Y. He, P. Luo, T. Shi, X. Chen, *J. Electrochem. Soc*., 163 (2016) D68.
39. T.R. Tamilarasan, U. Sanjith, M.S. Shankar, G. Rajagopal, T.R. Tamilarasan, U. Sanjith, M.S. Shankar, G. Rajagopal, *Wear*, 390 (2017) 385.